AIAA JOURNAL
Vol. 36, No. 7, July 1998

Boundary-Layer Receptivity to Transient Convected Disturbances

Anthony J. Dietz*
NASA Ames Research Center, Moffett Field, California 94035-1000

Previous work has shown that the boundary layer is receptive to acoustic and convected disturbances in regions where there is a rapid streamwise variation in the mean flow such as at the leading edge or at roughness elements or suction strips. Much of this work involved single-frequency, two-dimensional waves, and further studies are required to determine the effects of the broadband three-dimensional nature of turbulent fluctuations. An experimental investigation of the receptivity of a Blasius boundary layer to transient two-dimensional convected disturbances is presented here. A ribbon located upstream of a flat plate and aligned parallel to the plate leading edge was used to introduce disturbances into the freestream. Two-dimensional roughness elements distributed on the surface of the plate provided a receptivity site. Measurements of the boundary-layer response to single-frequency waves, pulses, and random noise disturbances are reported. Similar receptivity was measured for each of these disturbance types, showing that the broadband nature of transient disturbances does not affect the receptivity characteristics of the boundary layer and that linear superposition may be used to extend theories for single-frequency disturbances to applications involving broadband disturbances.

Nomenclature

E_w = hot-wire voltage
F = nondimensional frequency, $2\pi f\nu/U_\infty^2 \times 10^6$
f = dimensional forcing frequency
h = roughness height
R = boundary-layer Reynolds number, $\sqrt{(Re)} = \sqrt{(U_\infty x/\nu)}$
R_r = boundary-layer Reynolds number at the roughness location (branch I)
R_w = wire overheat ratio, set at 1.8 for these experiments
T_{fs} = freestream temperature
T_w = wire temperature calculated assuming $T_w = (R_w - 1)/\alpha_0$
U = time-averaged streamwise velocity
U_∞ = freestream velocity
u' = rms of streamwise velocity fluctuations
u'_{fs} = rms amplitude of the streamwise fluctuations at the boundary-layer edge ($\eta \cong 7$)
u'_{ts} = rms amplitude of the Tollmien–Schlichting (TS) wave
u'_{tsr} = rms amplitude of the TS wave at the roughness location (branch I)
x = streamwise distance from virtual leading edge
y = distance normal to plate surface
α_{ts} = TS wave number
α_{fs} = wave number of the streamwise fluctuations at the boundary-layer edge ($\eta \cong 7$)
α_0 = temperature coefficient of resistivity of the wire, 0.0036 at $T_0 = 293$ K
δ^* = boundary-layer displacement thickness
η = boundary-layer coordinate, $y/\sqrt{(2\nu x/U)}$
ν = dynamic viscosity

Introduction

An important link in the chain of events that leads to the transition of a laminar boundary layer to turbulence is the initial excitation and subsequent growth of Tollmien–Schlichting (TS) instability waves in the boundary layer. The process by which these waves are excited by freestream disturbances is known as receptivity. Acoustic disturbances, which propagate at the speed of sound, and vortical disturbances, which are transported by the freestream, cannot directly force the TS waves, which propagate at approximately one-third of the freestream velocity. The three have substantially different wavelengths, and a wavelength conversion mechanism is required for the boundary layer to be receptive to these disturbances.[1]

Goldstein[2] found that such a mechanism exists in the rapidly growing boundary layer in the leading-edge region. He and others also showed that wavelength conversion occurs in local regions with short-scale perturbations of the mean flow.[3–8] The temporal modulation of the short-scale, mean-flow perturbation by the longer-scale freestream disturbance can produce frequency wavelength combinations that match that of the TS wave.[9] This local mechanism is potentially more dangerous than the leading-edge mechanism as waves generated at the leading edge will decay considerably before reaching the lower branch of the neutral stability curve, whereas waves excited by a local mechanism near the lower branch will start to grow immediately. These analyses suggested that the following expression can be used to model the generation of TS waves by surface nonuniformities:

$$u'_{ts} = u'_{fs} F(\alpha_{ts} - \alpha_{fs}) \Lambda(F, R) \tag{1}$$

where $F(\alpha_{ts} - \alpha_{fs})$ is the spatial Fourier transform of the surface nonuniformity evaluated at a wave number equal to the difference between the TS wave number and the freestream wave number and $\Lambda(F, R)$ is an efficiency function that is a measure of the receptivity mechanism that is independent of the geometry.

Careful experiments by Saric et al.,[10] Wiegel and Wlezien,[11] and Zhou et al.[12] confirmed this theory for acoustic disturbances. Dietz[13,14] obtained similar confirmation for freestream vortical disturbances. He found that the vortical receptivity varied linearly with freestream forcing levels up to a forcing intensity (u'_{fs}/U_∞) of 1% and that it varied linearly with roughness height up to a nondimensional roughness height (h/δ^*) of 0.1. The variation with roughness geometry was also shown to be well modeled by the spatial Fourier transform, and the experimentally obtained efficiency function was in reasonable agreement with the results of calculations by Choudhari.[15]

However, both the theory and the experiments involved two-dimensional, single-frequency disturbances. Freestream turbulence consists of transient disturbances with a finite spanwise extent resulting in broad frequency and wave number spectra. In addressing receptivity to turbulence, the two-dimensional results must be extended to three dimensions, and the extent to which single-frequency results are applicable to broadband disturbances must be determined.

Presented as Paper 97-1962 at the AIAA 28th Fluid Dynamics Conference, Snowmass Village, CO, June 29–July 2, 1997; received Sept. 19, 1997; revision received March 20, 1998; accepted for publication March 20, 1998.

*National Research Council Research Associate, Fluid Mechanics Laboratory Branch; currently Senior Research Scientist, MCAT, Inc. Member AIAA.

Bruer et al.[16] measured local receptivity to broadband acoustic disturbances. They found that the receptivity mechanism remained linear with roughness height and number of roughness elements. However, a quantitative comparison between broadband and single-frequency receptivity measurements was not attempted.

An experiment investigating the receptivity of a Blasius boundary layer to transient two-dimensional convected disturbances is reported in this paper. Pulse and random noise disturbances are studied. The receptivity to these disturbances is compared with single-frequency measurements made in an identical configuration to determine the effect, if any, that the broadband nature of the transient disturbances has on the receptivity mechanism.

Experimental Technique

Experimental Setup

A schematic of the experimental setup is given in Fig. 1. The experiment was carried out in a low-speed indraft wind tunnel in the Fluid Mechanics Laboratory at the NASA Ames Research Center. Detailed descriptions of the facility and experimental technique were given in Refs. 13 and 14. The tunnel has a 0.4-m-square $\times$ 1.5-m-long test section and is powered by a centrifugal blower. A settling chamber with a honeycomb and eight seamless stainless-steel mesh screens followed by a 10:1 contraction introduces a high-quality flow into the test section. The flow nonuniformity is below 0.5%, the angularity is below 0.3 deg, and the turbulence intensity in the range of 3 Hz–10 kHz is below 0.07%.

A highly polished aluminum flat plate was used in the experiment. The plate was 1.2 m long and 0.0127 m thick with a 58:1 elliptic leading edge. It was mounted horizontally near the center of the test section. Care was taken to ensure the plate was adequately isolated from tunnel vibrations. The plate was set at a slight angle of attack to give a zero pressure gradient along its upper surface, and a 0.2-m flap at the rear of the plate was raised to bring the stagnation point back to the plate leading edge. In addition, a flexible ceiling was installed in the test section above the plate leading edge to minimize the adverse pressure gradient at the juncture of the leading edge and the plate.

A ribbon, 6.4 mm wide and 25 μm thick, mounted 0.58 m ahead of the plate leading edge was used to introduce disturbances into the freestream. The ribbon was stretched between two shafts mounted in sealed enclosures on either side of the test section. The thin ribbon under high tension had a natural frequency close to 400 Hz. Such a high frequency was required to prevent any ribbon vibration modes from corrupting the disturbance spectrum in the frequency range of interest. A single electromagnetic shaker was used to drive the shafts. Roughness elements 25.4 mm wide and 100 μm thick were applied to the plate in the vicinity of the first branch of the neutral stability curve to provide a receptivity site. The elements were formed by laminating two strips of 50-μm-thick polyester tape. Two roughness configurations were investigated: a single roughness located at $R = 613$ and distributed roughness consisting of 10 strips that were evenly spaced at 50.8-mm intervals, with 4 strips in front of the single element and 5 behind it.

Streamwise velocity measurements were made using two single-wire Dantec 5-μm-diam hot wires. The primary hot wire was supported by a three-axis traverse housed in a sealed enclosure above the test section. A streamlined sting passed from the traverse enclosure, through a sealed slot, and into the test section where the hot wire was mounted at the tip of a 0.12-m extension tube to ensure it was free from any pressure-gradient effects associated with the sting. Care was taken to minimize any vortex shedding from the sting or the slot that could corrupt the measurements. A second hot wire was used as a reference for phase measurements. It was mounted on a fixed sting at the streamwise location of the single roughness. The wire was offset 0.05 m in the spanwise direction from the tunnel centerline and positioned close to the upper edge of the ribbon wake. Freestream pressure and temperature were measured using a pitot tube and a platinum resistance thin film detector mounted on the traverse sting just above the primary hot wire. Atmospheric pressure was regularly updated from a digital barometer. All analog signals were acquired simultaneously by a high-speed, 15-bit, Tustin A/D converter and then transferred to a Micro VAX II computer.

Measurement Technique

The hot wires were always calibrated in the same reference positions against freestream velocity determined from the pitot tube. The temperature sensitivity of the hot wire was taken into account by assuming $U = f[E_w/(T_w - T_{\rm fs})^{1/2}]$. An eight-point, fourth-order polynomial fit was used for the calibration. The streamwise velocity fluctuation rms values were estimated from the product of the ac-coupled rms voltage and the local slope of the calibration curve, $\mathrm{d}U/\mathrm{d}E_w = 1/(T_w - T_{\rm fs})^{1/2} f'[E_w/(T_w - T_{\rm fs})^{1/2}]$. The wires were calibrated before every set of measurements, and the calibration was checked on completion of each set. If the calibration was out of tolerance, the measurements were repeated. The absolute accuracy of the hot-wire velocity measurements in the freestream was estimated to be $\pm 2\%$. This was largely due to the estimated accuracy of the pitot pressure measurements as the standard error of the hot-wire calibrations was typically 0.3% and the drift of the hot-wire velocity estimate (measured after each data set at the reference location) was typically less than 1%.

Spectral measurements were performed with a HP 3665A Dynamic Signal Analyzer. Narrow-band velocity amplitudes were determined from a power spectrum of the primary hot-wire signal, and the corresponding phase was determined from a cross spectrum of signals from the primary and reference hot wires. A flat-top window was used for the continuous and random disturbances, and a uniform window was used for the pulse disturbance. Both windows had bandwidths of approximately 2 Hz. The spectra presented here were the result of 100 ensemble averages. Phase-locked-averaged time traces are also presented. These result from some 200 averages of 512 point records sampled at 1600 Hz and triggered from the reference hot-wire signal.

Experimental Conditions

The experimental conditions were the same as those used in the author's earlier study of receptivity to continuous single-frequency convected disturbances.[13,14] These parameters were chosen to give maximum receptivity with tape of a certain width positioned at branch I and maximum amplification from this site to the downstream measurement position. The downstream position was fixed at 0.7 m as side wall contamination was unacceptable aft of this

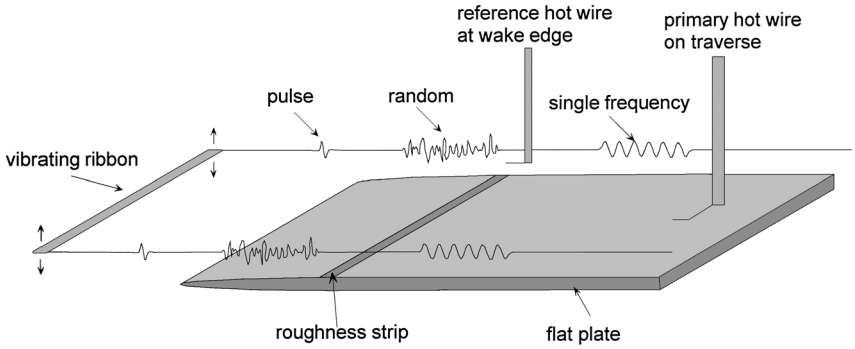

Fig. 1 Schematic of test setup showing the pulse, random, and single-frequency disturbances generated by the vibrating ribbon.

position. For standard 25.4-mm tape, the optimum experiment parameters were $F = 50$ and $R_r = 613$, giving $U = 17$ m/s and $f = 157$ Hz at a reference temperature of 288 K and a reference dynamic viscosity of 1.455×10^{-5} m^2 s^{-1}. The experiment was controlled to maintain a constant R and F by adjusting the freestream velocity and the ribbon forcing frequency as the flow temperature and the atmospheric pressure varied.

Mean Flow

Accurate characterization of the boundary-layer mean flow was important because measurements of the TS waves were made at the downstream measurement position where the exponential growth of the waves had increased their amplitudes to measurable levels. It was then necessary to use amplification factors calculated using linear stability theory to determine the wave amplitude at the receptivity site, and these factors are very sensitive to pressure gradients. After careful adjustment, the streamwise variation in the pressure coefficient along the plate for $R > 520$ was reduced to within $\pm 0.2\%$ of the mean value. The variation was less than $\pm 0.1\%$ for $R > 600$. The leading-edge region $R < 520$ had a strong favorable pressure gradient, but this was considered to be beneficial as it served to dampen any instabilities excited upstream of the receptivity site at $R = 613$.

The Blasius characteristics of the boundary layer were confirmed from mean streamwise velocity profiles recorded at a number of x stations. The shape factors calculated from these profiles were consistently within 1% of the Blasius value of 2.59. A virtual origin of 0.025 m was calculated from these profiles, $x_{vo} = \delta^{*2} U_\infty / (1.728\nu)$. All x data reported in this paper are referenced to this virtual origin. An indication of the quality of the boundary layer and of the virtual origin estimate is given in Fig. 2, where the measured mean flow profiles at a number of x stations are plotted using a nondimensional height η based on the x_{vo} estimate of 0.025 m. The profiles all match the theoretical self-similar Blasius profile, which is also included in Fig. 2.

Ribbon Wake

The characteristics of the wake from the vibrating ribbon and its effect on the boundary layer were carefully measured to establish the input to the receptivity process. These measurements were reported in detail by Dietz.[13,14] The ribbon was installed some 0.58 m (91 ribbon chords) ahead of the plate leading edge to allow the wake velocity deficit and any coherent wake structures time to decay. Also, with a small wake deficit, the wake disturbances generated by vibrating the ribbon should convect at a speed close to that of the freestream. The ribbon wake was positioned close to the edge of the boundary layer so that there would be a strong boundary-layer response to the convected wake disturbances but sufficiently high

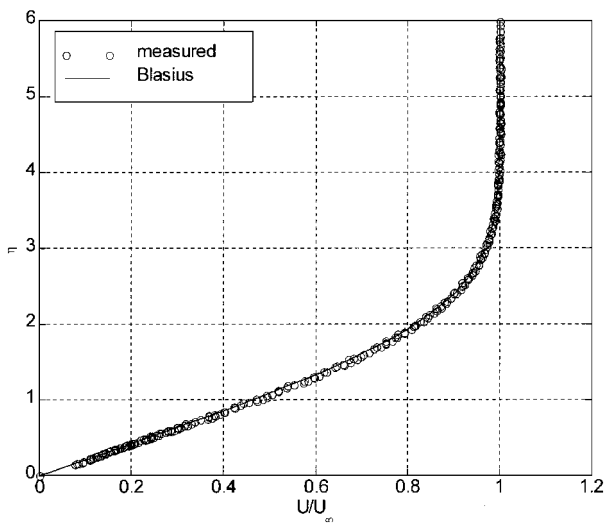

Fig. 2 Variation of the mean streamwise velocity through the boundary layer at 12x stations from $R = 630$ to 900 compared with the theoretical Blasius profile.

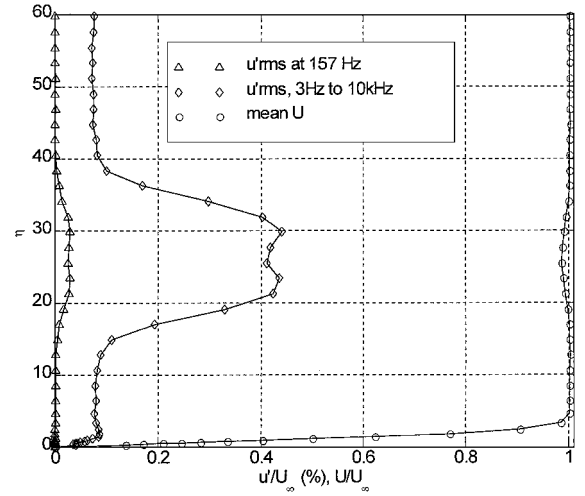

Fig. 3 Profile of the streamwise velocity in the boundary layer and the wake behind the stationary ribbon measured at $R = 633$. Broadband, narrow-band, and mean velocity measurements are shown.

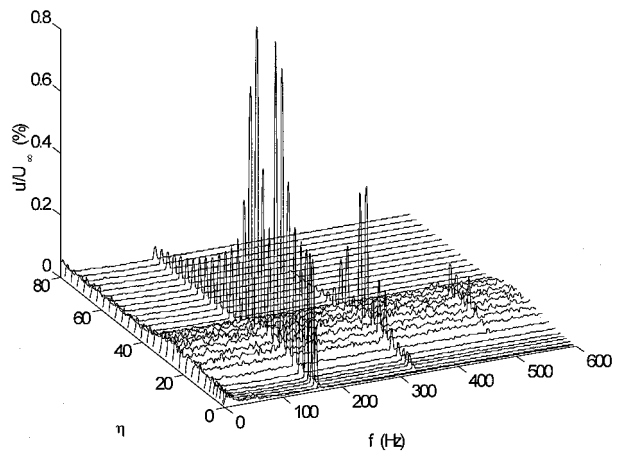

Fig. 4 Streamwise velocity spectra recorded in the boundary layer and the vibrating ribbon wake; $R = 633$ and $F = 50$.

to prevent any excitation of the boundary layer by turbulent fluctuations in the wake. Profiles of the mean streamwise velocity and the rms velocity fluctuations in the boundary layer and the wake from the stationary ribbon are given in Fig. 3. The maximum velocity deficit in the wake is less than 2% of the freestream velocity, and it is located well above the edge of the boundary layer. Both the broadband and narrow-band fluctuation levels plotted in Fig. 3 decay to negligible levels by the edge of the boundary layer, and there is no detectable excitation of the boundary layer by the wake turbulence.

The characteristics of disturbances produced by ribbon vibration are shown in the spectra recorded in the wake and the boundary layer with the ribbon vibrating at the reference frequency of 157 Hz (Fig. 4). Fluctuations at the forcing frequency dominate the disturbance profile, and although the wake turbulence remains localized above the boundary layer, the disturbance fluctuations at the forcing frequency extend into the potential flow region beyond the wake and excite the boundary layer. There is some energy present in the second and third harmonics, but sufficient ribbon tension has reduced these to acceptable levels. These measurements demonstrate that the wake from a vibrating ribbon is an effective way to excite a boundary layer with single-frequency convected disturbances. In the next section the responses of the boundary layer to disturbances excited by pulse and random ribbon vibrations are investigated.

Results

Response to a Transient Pulse

The first transient disturbance analyzed was a pulse generated by forcing the ribbon with a single sine cycle at a frequency of 157 Hz.

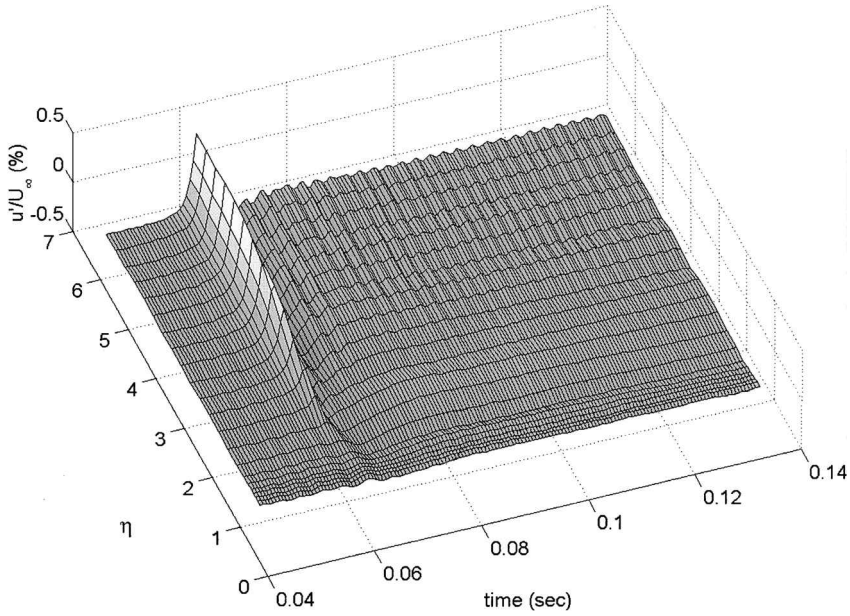

Fig. 5 Boundary-layer response to a pulse disturbance: phase-locked-averaged time records of the streamwise velocity fluctuations measured at a number of heights through the layer; single roughness at $R = 613$ and hot wire positioned at $R = 640$.

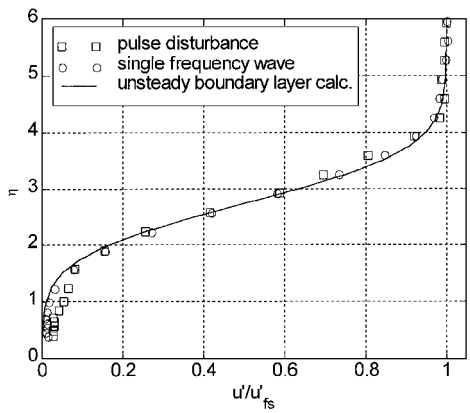

Fig. 6 The rms amplitude of the convected pulse and single-frequency disturbances in the boundary layer compared with the results of an unsteady boundary-layer calculation.[15,18]

Such a pulse should excite a broad range of frequencies in the boundary layer. This is essentially an application of the classical impulse or bump test used to determine the natural frequencies of a structure. Another useful advantage of this technique, pointed out by Saric et al.,[17] is that as the TS wave propagates at approximately one-third of the freestream velocity, it lags behind the convected disturbance, and the two may be analyzed separately in downstream measurements.

The boundary-layer response to the pulse disturbance is shown in Fig. 5, where phase-locked-averaged time records of the streamwise velocity at a range of heights in the boundary layer are plotted. The hot wire was located at $R = 640$, which was just downstream of the single-roughness receptivity site. The 0.06-s time delay between the pulse displacement of the ribbon and the pulse disturbance at the hot wire matches that expected for a disturbance convected at the freestream speed. The pulse has remained compact in the streamwise direction, giving the desired short-duration excitation. In Fig. 6, the amplitude of the pulse through the boundary layer is compared with the profile measured with single-frequency excitation. The boundary-layer response is similar in each case. The measured profiles also agree well with results from an unsteady boundary-layer calculation with streamwise forcing as the upper boundary condition.[15,18] The disturbance energy is confined to the outer part of the boundary layer, and the fluctuations are rapidly damped toward the wall. With similar disturbance profiles, the input into the receptivity process is similar, and so a comparison between the receptivity to these transient and continuous disturbances is valid.

The response of the boundary layer measured at the downstream measurement location, $R = 900$, is shown in Fig. 7. A TS wave packet can now be seen, lagging the pulse with its maximum amplitude occurring close to the wall as expected for a TS eigenvector. The wave packet was not detectable in Fig. 5, which was measured at $R = 640$, just downstream of the roughness element, but the exponential growth of the waves resulted in an easily detected wave packet at $R = 900$. The N factor between these two locations is approximately 2 for $F = 50$, which corresponds to a sevenfold increase in the amplitude over this distance. The propagation speed of the TS packet from the roughness strip to the measurement location, calculated assuming the pulse disturbance was convected from the ribbon to the roughness strip at the freestream velocity, is approximately one-third of the freestream velocity. This is a close match to the speed predicted by linear stability theory for waves in this frequency range. Analysis of the wave propagation times also demonstrates that the wave packet was generated by the convected pulse because a packet generated by an acoustic or vibration disturbance would have arrived at an earlier time.

The response of the boundary layer with an array of 10 roughness elements on the plate is shown in Fig. 8. A much larger wave packet has been generated by the distributed roughness. The mode shape of the TS wave is clear, and the 180-deg phase shift characteristic of TS waves can be seen in the outer part of the layer where the wave amplitude drops to zero. The roughness elements were spaced to match the resonant condition where the wall wave number equals the difference between the TS and the freestream wave numbers. At this spacing, resonant TS waves generated at successive roughness strips are in phase and add constructively. The profile of the maximum amplitude in the packet is plotted in Fig. 9, where it is compared with the profile of a TS wave excited by continuous single-frequency forcing and also with the TS eigenvector of linear stability theory, calculated using the e$^{\text{Malik}}$ quasiparallel spatial stability code.[19] There is good agreement between the profiles.

Response to Random Excitation

Just as white noise can be used to determine the transfer function of an amplifier, a random noise input was used as a second way to determine the boundary-layer response to broadband disturbances. Driving the ribbon with a random noise source from the spectrum analyzer did successfully introduce a broadband disturbance into the freestream. In Fig. 10 the spectrum of this disturbance is compared with that of the pulse disturbance. The large spike at 375 Hz is the

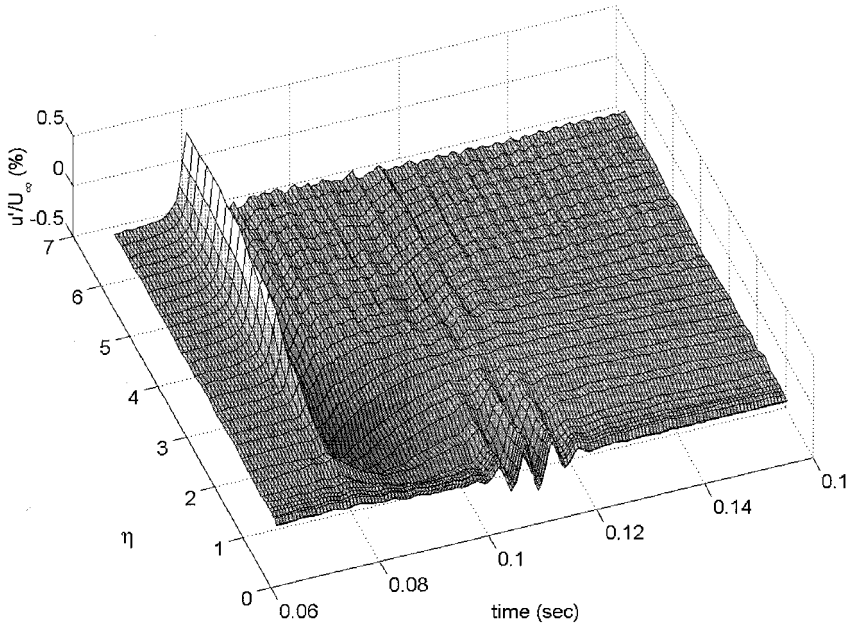

Fig. 7 Boundary-layer response to a pulse disturbance: phase-locked-averaged time records of the streamwise velocity fluctuations measured at a number of heights through the layer; single roughness at $R = 613$ and hot wire positioned at $R = 900$.

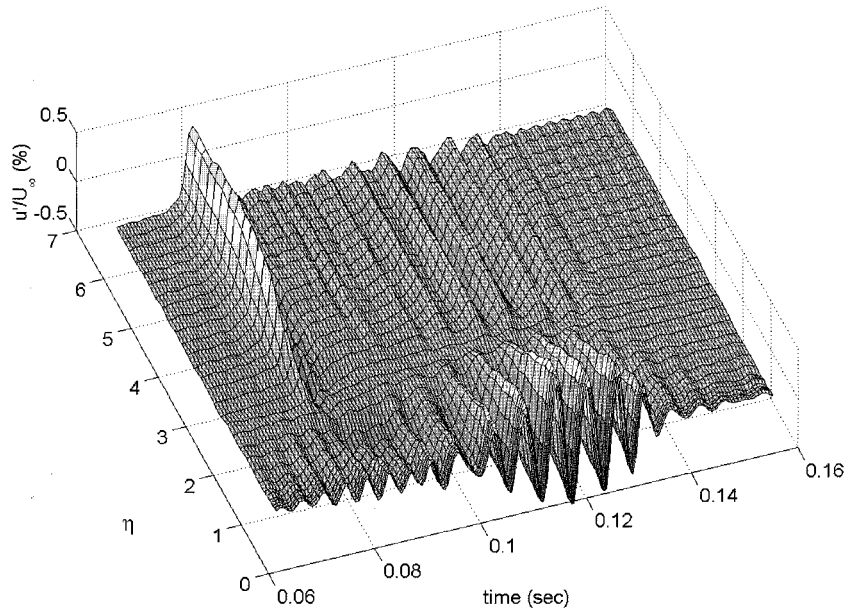

Fig. 8 Boundary-layer response to a pulse disturbance: phase-locked-averaged time records of the streamwise velocity fluctuations measured at a number of heights through the layer; array of 10 roughness elements on the plate; hot wire positioned at $R = 900$.

natural frequency of the ribbon. The different amplitude distributions of the two spectra should provide a good test of the linearity of the boundary-layer response.

The response of the boundary layer to the random noise and pulse disturbances is shown in Fig. 11 for the single roughness case and in Fig. 12 for distributed roughness. These spectra were recorded at the downstream measurement position, $R = 900$, with the hot wire positioned in the boundary layer at the height of the maximum TS wave amplitude. Each spectrum is normalized by the u'_{fs} spectrum measured at the edge of the boundary layer at the roughness location. This normalization accounts for any differences in the amplitude or frequency distribution of the forcing and has the added advantage of removing any effects due to the bandwidth of the spectral measurements as both TS and freestream spectra are measured with the same parameters. The spectra measured with no roughness on the plate are also included in these figures to demonstrate the significant increase in wave amplitude due to the roughness. The single-roughness spectrum has a maximum around 200 Hz, which is close to the frequency of the most amplified TS wave at this Reynolds number. The distributed-roughness spectrum has a maximum at a lower frequency of 170 Hz. This is a result of the tuning effect of the single wave number roughness array. The wave amplitudes for the distributed roughness are an order of magnitude greater than those generated by the single roughness.

Two-Dimensional Receptivity Results

To obtain a valid comparison between the results for the pulse, random, and single-frequency disturbances, the three measurements for a particular roughness configuration were made consecutively in closely spaced runs with no alterations to the experimental setup.

The single-frequency TS amplitudes were obtained by subtracting the complex amplitudes measured with no roughness from the amplitudes measured with roughness. This technique was not possible for the broadband measurements, which had no phase information. However, the broadband freestream disturbance and the TS wave packets excited at the roughness are essentially uncorrelated,

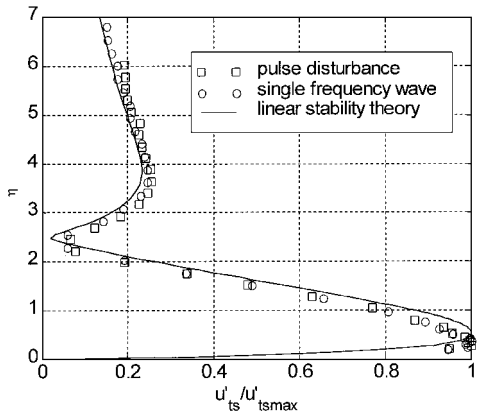

Fig. 9 Measured profile of the TS eigenvector excited by pulse and single-frequency disturbances at distributed roughness compared with e^{Malik} calculations,[19] both normalized by the maximum amplitude near the wall; $R = 900$.

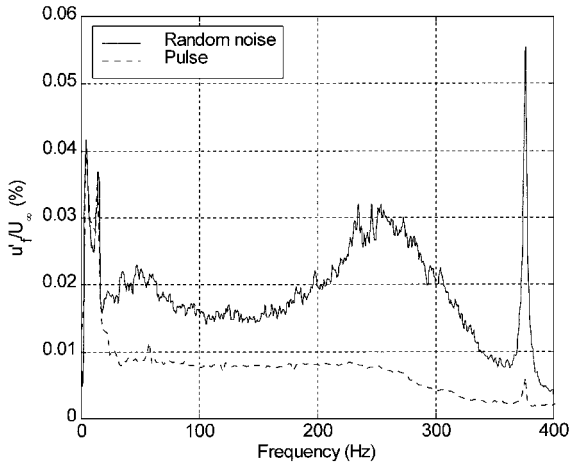

Fig. 10 Spectra of the streamwise velocity for random noise and pulse excitation of the ribbon; hot wire positioned at $R = 630$ and $\eta = 8$.

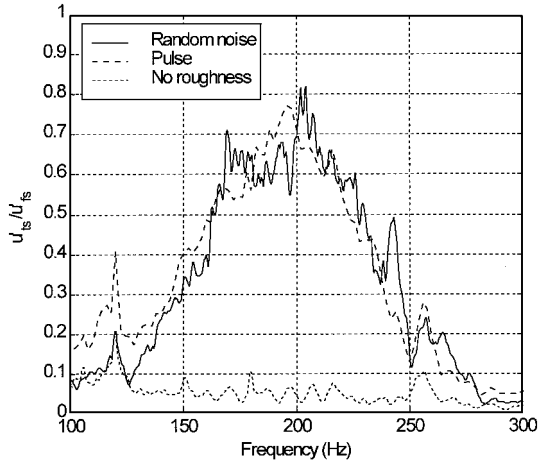

Fig. 11 Response of the boundary layer with a single roughness element at $R = 613$ to random noise and pulse disturbances; hot wire positioned at $R = 900$ and $\eta = 0.5$.

and so the TS amplitude spectrum was determined by subtracting the no-roughness power spectrum from the spectrum measured with roughness. (The subtraction of power spectra was suggested by Bradshaw[20] for removing uncorrelated noise from a signal.)

Stability calculations were then used to decouple the receptivity process from the subsequent growth of the waves, which is well described by solutions of the Orr–Sommerfeld equation of linear stability theory. The e^{Malik} code was used to calculate the growth rate of each TS eigenvalue for the R, F parameter space being studied.

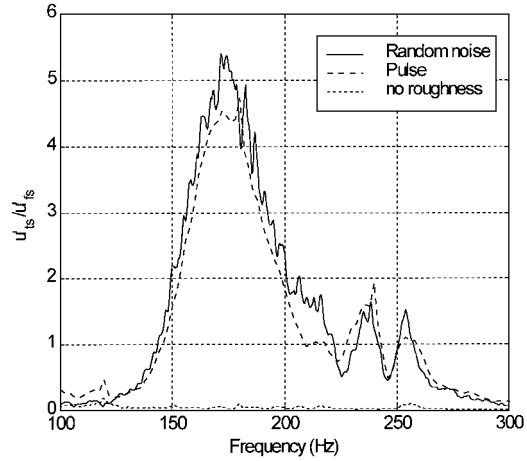

Fig. 12 Response of the boundary layer with distributed roughness to random noise and pulse disturbances; hot wire positioned at $R = 900$ and $\eta = 0.5$.

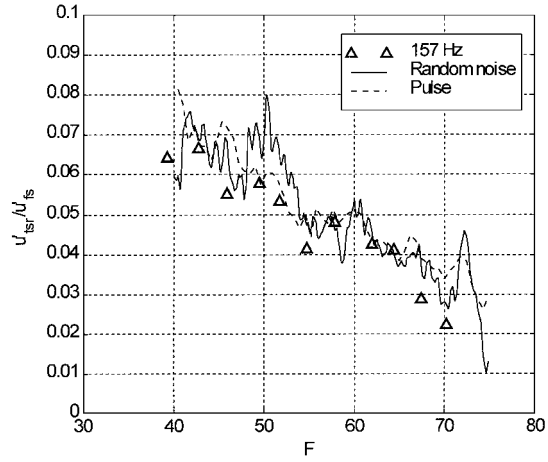

Fig. 13 Boundary-layer receptivity at a single-roughness element for three disturbance types.

The N factor for each frequency in the spectrum was determined by integrating the growth rate between the roughness location and the measurement location:

$$N(F) = \ln\left(\frac{u'_{ts}}{u'_{tsr}}\right) = \int_{R_r}^{R} -2\alpha_i(F, R)\,\mathrm{d}R \qquad (2)$$

These N factors were then used to determine the TS wave amplitudes at the roughness location from the amplitudes measured downstream. The results are presented in terms of a receptivity coefficient defined as u'_{tsr}/u'_{fs}.

The receptivity results for the random noise and pulse disturbances are compared with the single-frequency results in Fig. 13 for a single roughness element and in Fig. 14 for an array of roughness elements. Very good agreement between the three excitation types is seen in both plots. This demonstrates that, at least for two-dimensional waves, it is valid to consider the response to a broadband disturbance as the superposition of the response to individual frequency components. Current linear receptivity theories may therefore be applied with confidence to transient disturbances. The results also validate the spectral approach used to determine the receptivity coefficient and show that the use of pulse or random disturbances is a rapid way to determine the frequency dependence of this coefficient.

A comparison of the single-roughness response measured downstream (Fig. 11) with the receptivity coefficient (Fig. 13) shows that the frequency tuning in the downstream response is due to the frequency-dependent growth of the waves. The receptivity coefficient in Fig. 13 decreases monotonically with frequency. If the geometry dependence is removed, the resulting efficiency factor

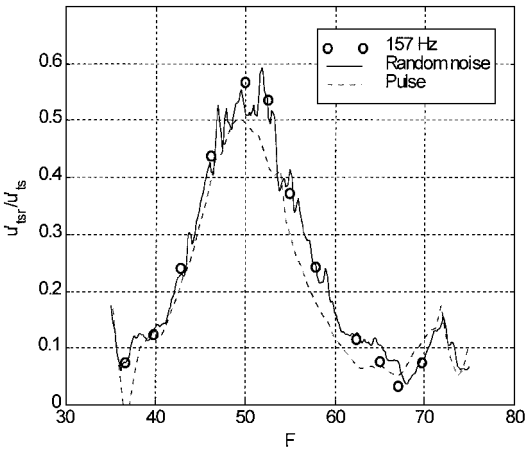

Fig. 14 Boundary-layer receptivity at distributed roughness for three disturbance types.

shows only a slight decrease with frequency,[14] a trend that matches the results of Choudhari.[15] In contrast, the receptivity to distributed roughness exhibits the highly tuned response predicted by Crouch,[8] as waves at the resonant wave number reinforce and those away from the resonant wave number interfere. The magnitude of the receptivity coefficient for distributed roughness is an order of magnitude greater than that for single roughness. This result also agrees with the theoretical calculations of Crouch,[8] who calculated the receptivity for a wavy wall to be 10 times that of a Gaussian hump.

Conclusions

The receptivity of a Blasius boundary layer with two-dimensional roughness elements to broadband transient convected disturbances was measured as a first step toward validating the use of single-frequency receptivity theories with real-world disturbances. Two-dimensional pulse and random disturbances were investigated. The interaction of the freestream pulse disturbance with a single roughness strip excited a TS wave packet that lagged the freestream disturbance due to its lower propagation speed. A larger packet was excited with an array of distributed roughness elements on the plate. The amplitudes in the spectra of these packets and of the waves excited by the random noise disturbance were compared with the amplitudes of waves excited by continuous single-frequency disturbances. The receptivity was shown to be the same in each case, demonstrating that receptivity to a broadband disturbance may be modeled as the linear superposition of the receptivity to discrete frequencies. In addition, the use of pulse or random noise disturbances proved to be an effective way of rapidly determining the variation of the receptivity coefficient with frequency. The receptivity measured with this technique exhibited trends that agreed with calculations made by previous researchers using finite Reynolds number receptivity theories.

Acknowledgments

The author was supported by a National Research Council research associateship for the duration of this work. The advice and support of S. Davis is gratefully acknowledged. In addition, the experiment benefited from the work and advice of M. Choudhari and from a discussion with Ed Kerschen. The author also wishes to thank M. Malik for the use of his stability code.

References

[1]Reshotko, E., "Boundary-Layer Stability and Transition," *Annual Review of Fluid Mechanics*, Vol. 8, 1976, pp. 311–349.

[2]Goldstein, M. E., "The Evolution of Tollmien–Schlichting Waves Near a Leading Edge," *Journal of Fluid Mechanics*, Vol. 127, 1983, pp. 59–81.

[3]Goldstein, M. E., "Scattering of Acoustic Waves Into Tollmien–Schlichting Waves by Small Streamwise Variations in Surface Geometry," *Journal of Fluid Mechanics*, Vol. 154, 1985, pp. 509–529.

[4]Zavol'skii, N. A., Reutov, V. P., and Ryboushkina, G. V., "Excitation of Tollmien–Schlichting Waves During the Scattering of Acoustic and Vortex Perturbations in a Boundary Layer on a Wavy Surface," *Zhurnal Prikladnoi Mekhaniki i Tekhnicheskoi Fiziki*, No. 3, 1983, pp. 79–86 (in Russian).

[5]Ruban, A. I., "On the Generation of Tollmien–Schlichting Waves by Sound," *Izvestiya Akademii Nauk SSSR, Mekhanika Zhidkosti i Gaza*, Vol. 19, No. 5, 1984, pp. 44–52 (in Russian); translation in *Fluid Dynamics*, Vol. 19, March 1985, pp. 709–716.

[6]Kerschen, E. J., "Linear and Non-Linear Receptivity to Vortical Free-Stream Disturbances," *Boundary Layer Stability and Transition to Turbulence*, edited by D. C. Reda, H. L. Reed, and R. Kobayashi, ASME FED-Vol. 114, American Society of Mechanical Engineers, New York, 1991, pp. 43–48.

[7]Choudhari, M., and Streett, C. L., "Theoretical Prediction of Boundary Layer Receptivity," AIAA Paper 94-2223, June 1994.

[8]Crouch, J. D., "Theoretical Studies on the Receptivity of Boundary Layers," AIAA Paper 94-2224, June 1994.

[9]Kerschen, E. J., "Boundary Layer Receptivity Theory," *Applied Mechanics Reviews*, Vol. 43, No. 5, Pt. 2, 1990, pp. S152–S157.

[10]Saric, W. S., Hoos, J. A., and Radeztsky, R. H., "Boundary-Layer Receptivity of Sound with Roughness," *Boundary Layer Stability and Transition to Turbulence*, edited by D. C. Reda, H. L. Reed, and R. Kobayashi, ASME FED-Vol. 114, American Society of Mechanical Engineers, New York, 1991, pp. 17–22.

[11]Wiegel, M., and Wlezien, R., "Acoustic Receptivity of Laminar Boundary Layers over Wavy Walls," AIAA Paper 93-3280, July 1993.

[12]Zhou, M. D., Liu, D. P., and Blackwelder, R. F., "An Experimental Study of Receptivity of Acoustic Waves in Laminar Boundary Layers," *Experiments in Fluids*, Vol. 17, No. 1/2, 1994, pp. 1–9.

[13]Dietz, A. J., "Distributed Boundary Layer Receptivity to Convected Vorticity," AIAA Paper 96-2083, June 1996.

[14]Dietz, A. J., "Local Boundary-Layer Receptivity to Convected Vorticity," *Journal of Fluid Mechanics* (submitted for publication).

[15]Choudhari, M., "Boundary-Layer Receptivity to Three-Dimensional Unsteady Vortical Disturbances in Free Stream," AIAA Paper 96-0181, Jan. 1996.

[16]Breuer, K. S., Dzenitis, E. G., Gunnarsson, J., and Ullmar, M., "Linear and Nonlinear Evolution of Boundary Layer Instabilities Generated by Acoustic-Receptivity Mechanisms," *Physics of Fluids*, Vol. 8, No. 6, 1996, pp. 1415–1423.

[17]Saric, W. S., Wei, W., Rasmussen, B. K., and Krutcoff, T. K., "Experiments on Leading-Edge Receptivity to Sound," AIAA Paper 95-2253, June 1995.

[18]Davis, S. S., "Wave Excitation in an Unsteady Boundary Layer," AIAA Paper 97-1833, June 1997.

[19]Malik, M. R., "e^{Malik}: A New Spatial Stability Analysis Program for Transition Prediction Using the e^N Method," High Technology Corp., HTC-8902, Hampton, VA, March 1989.

[20]Bradshaw, P., *An Introduction to Turbulence and its Measurement*, 1st ed., Pergamon, Oxford, England, UK, 1971, pp. 146–148.

S. Glegg
Associate Editor